

Supplementary Information

i-CRISPR: a personalized cancer therapy strategy through cutting cancer-specific mutations

Junfeng Jiang^{#1,4}, Yuanyuan Chen^{#2}, Li Zhang^{#3}, Qishu Jin⁵, Liujun Wang¹, Sha Xu¹, Kexin Chen⁶, Li Li¹, Tao Zeng^{1,7}, Xingfei Fan¹, Tingting Liu², Jiayi Li⁸, Jinjiang Wang⁸, Chaofeng Han^{*1}, Fu Gao^{*2}, Yanyong Yang^{*2}, Yue Wang^{*1,4}

#Authors contributed equally to this work.

1. Histology and Embryology Department, Naval Medical University, Shanghai, 200433, China
2. Department of Radiation Medicine, Faculty of Naval Medicine, Naval Medical University, 800, Xiangyin Road, 200433, Shanghai, P.R. China;
3. Department of Pathology, Faculty of Medical Imaging Laboratory of Medical Imaging, Naval Medical University, Shanghai, 200433, China
4. Shanghai Key Laboratory of Cell Engineering, Naval Medical University, Shanghai, 200433, China.
5. Department of Histology and Embryology, Harbin Medical University, Harbin 150086, China
6. Department of Plastic Surgery, The First Affiliated Hospital of Naval Medical University, Shanghai 200433, China
7. The 901th Hospital of PLA Joint Logistic Support Force, HeFei, 230031, China
8. Department of Oncology, Tongren Hospital, Shanghai Jiao Tong University School of Medicine, Shanghai, 200336, China

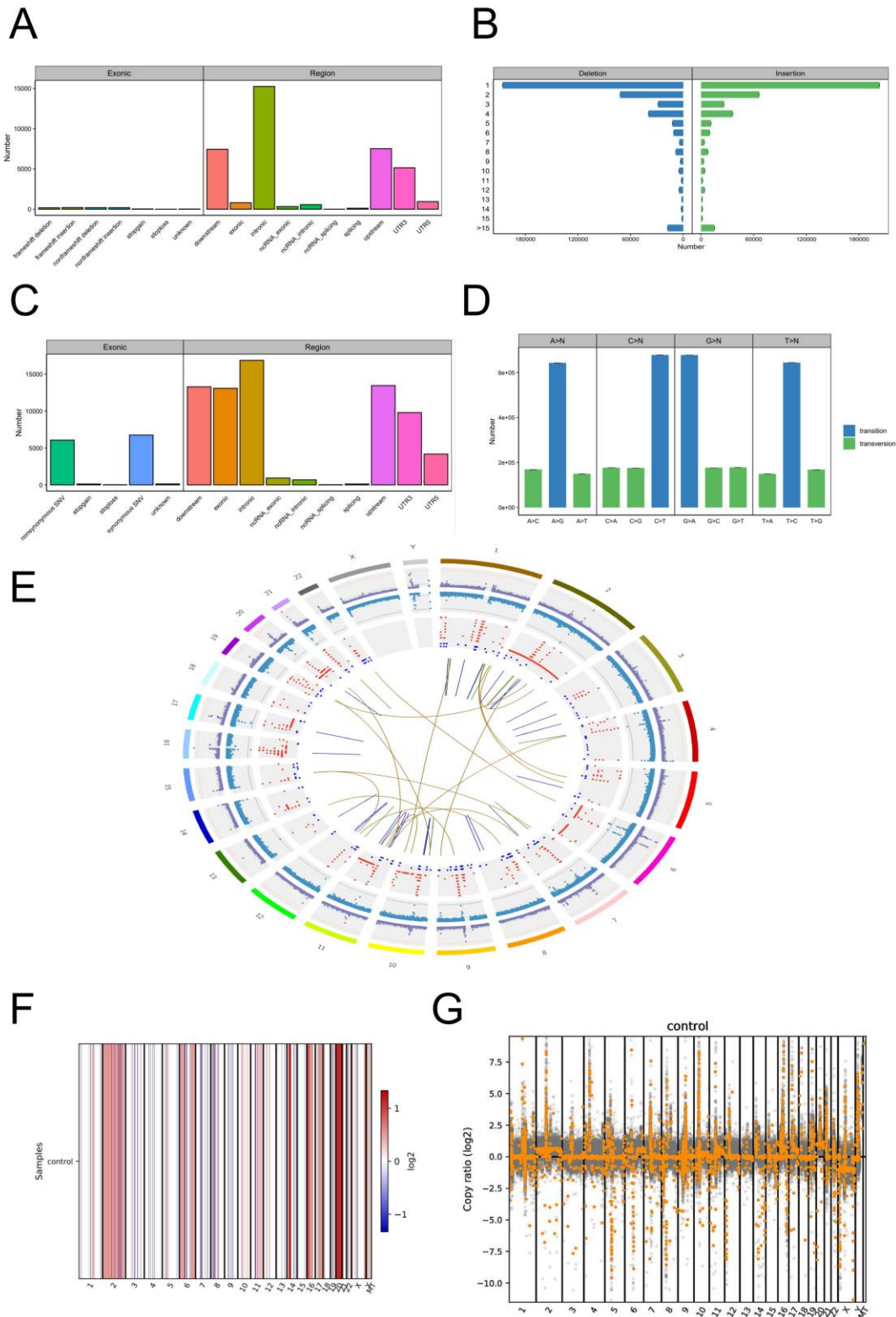
*Corresponding author:

Yue Wang, wangyuesmmu@163.com; Yanyong Yang, yvyang2010@163.com;

Fu Gao, gaofusmmu@163.com; Chaofeng Han, hcf@immunol.org;

Address: 800, Xiangyin Road, 200433, Shanghai, P.R. China.

33 **1. Supplementary figures**



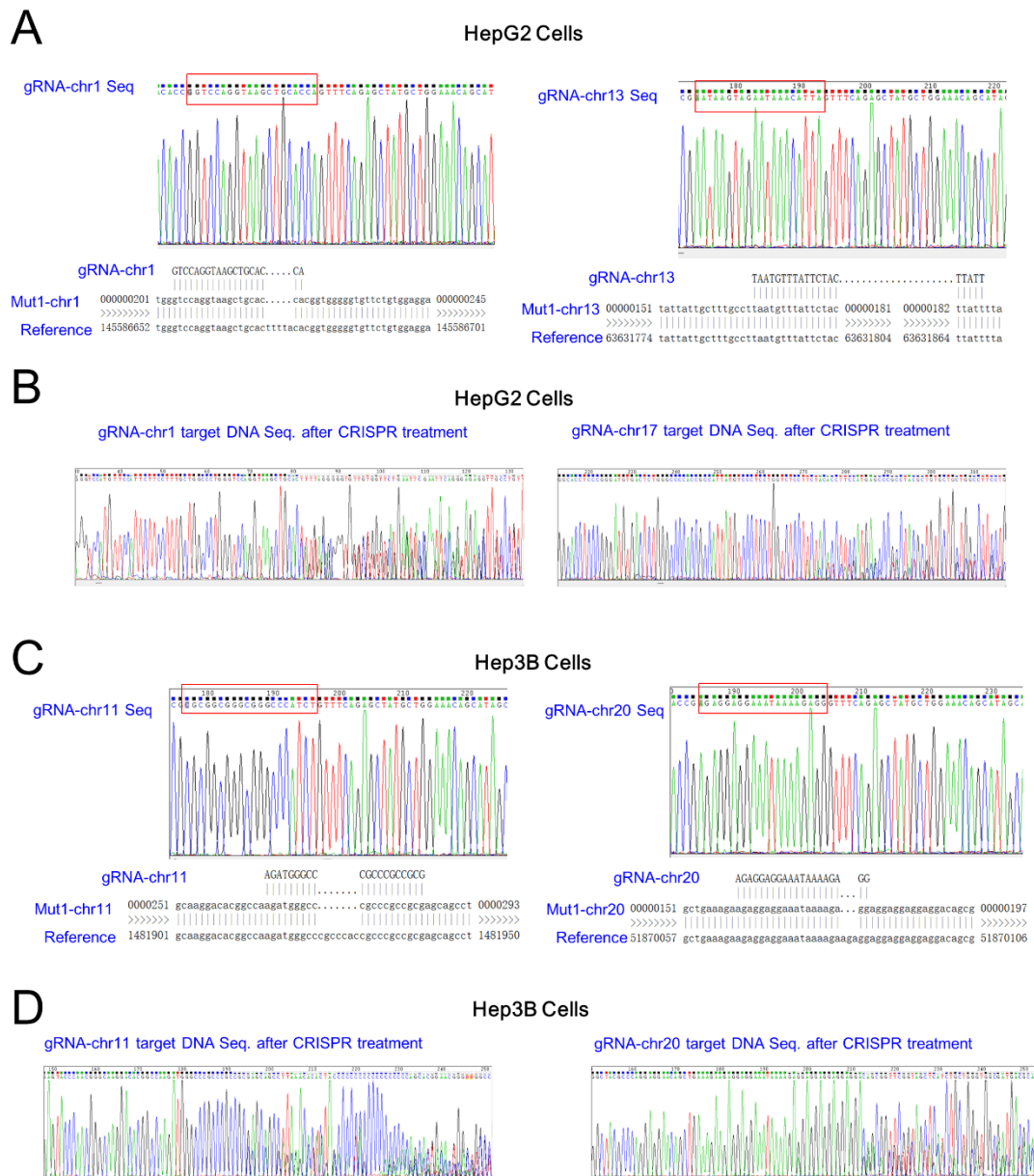
34

35 **Fig. S1 WGS results in HepG2.**

36 **A.** The WGS (whole genome sequencing) results showed the distribution of
 37 indel (insertion or deletion mutations) on different DNA segments in HepG2
 38 cells.

39 **B.** The indel substitution in HepG2 cells discovered by WGS.

40 **C.** The WGS results showed the distribution of SNV on different DNA segments
 41 in HepG2 cells.
 42 **D.** The SNV substitution in HepG2 cells discovered by WGS.
 43 **E.** A Circos plot showing the genomic landscape of mutations (including SNVs,
 44 Indels, CNVs, and gene fusions) in HepG2 cells discovered by WGS. The outer
 45 ring shows chromosome ideograms. The bars along each inner ring represent
 46 mutation events.
 47 **F-G.** Copy-number variation (CNV) distribution on chromosomes in our cultured
 48 HepG2 cells discovered by WGS.
 49
 50



51

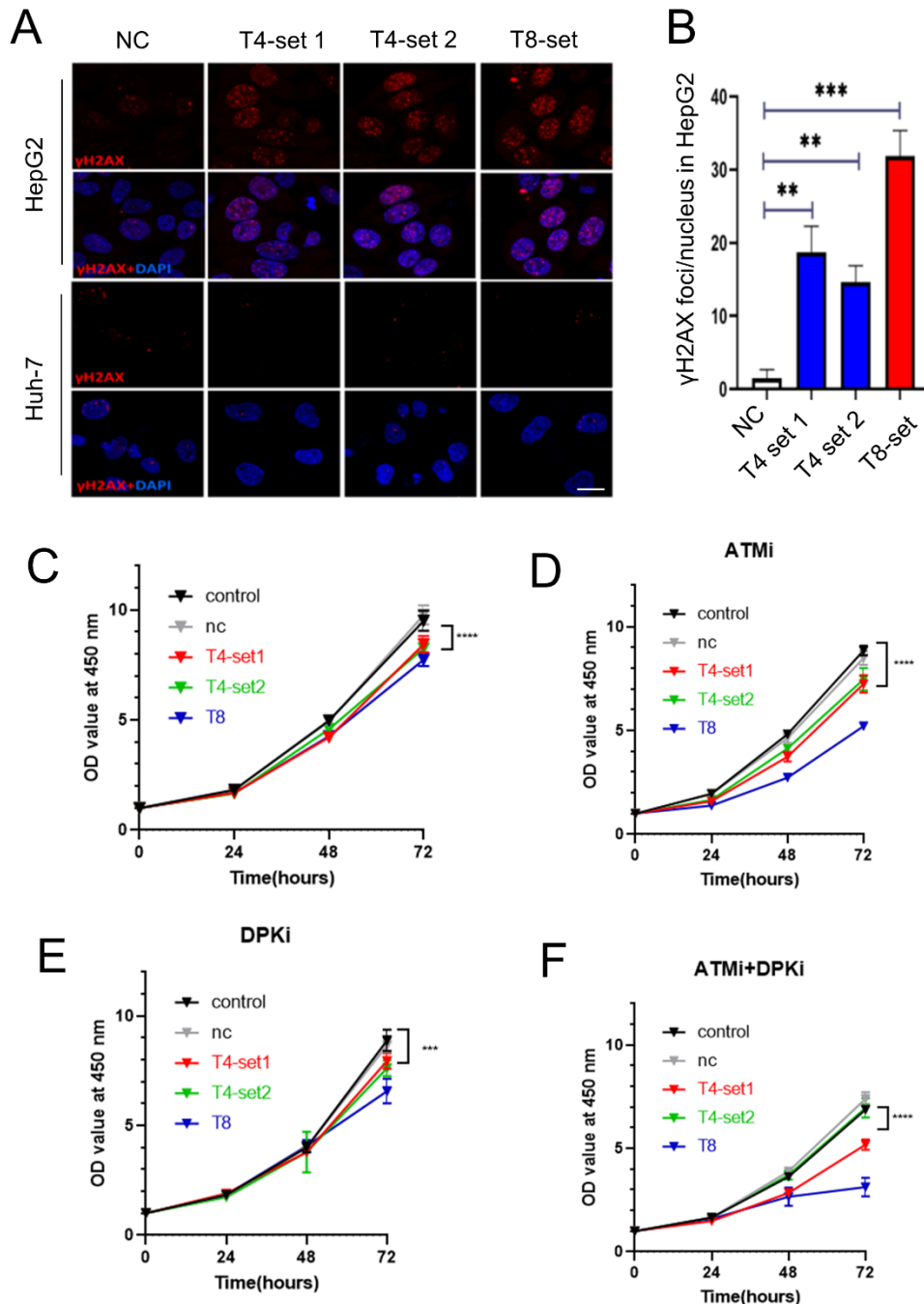
52 **Fig. S2 Representative Sanger sequencing results of gRNA-expression**
 53 **vectors and their targeting sites in HepG2 and Hep3B.**

54 **A.** The representative sequences of the designed gRNA-expression vectors
55 which only target mutated DNA sites in hepatocellular carcinoma (HCC) cell line
56 HepG2.

57 **B.** Representative Sanger sequencing results of the PCR product showed the
58 emergence of abnormal peaks at the gRNA targeting site, which indicated the
59 designed CRISPR could successful induce DSBs in HePG2 cells. This
60 experiment was used to verify the CRISPR cutting efficiency. The cells only
61 received CRISPR treatment, but not DSB repair inhibitors (DSBri) treatment.

62 **C.** The representative sequences of the designed gRNAs which only target
63 mutated DNA sites in HCC cell line Hep3B.

64 **D.** Representative Sanger sequencing results of the PCR product showed the
65 emergence of abnormal peaks at the gRNA targeting site, which indicated the
66 designed CRISPR could successful induce DSBs in HeP3B cells.



67

68 **Figure S3 The "i-CRISPR" strategy could induce DSBs and cell death**
 69 **in HepG2 cells.**

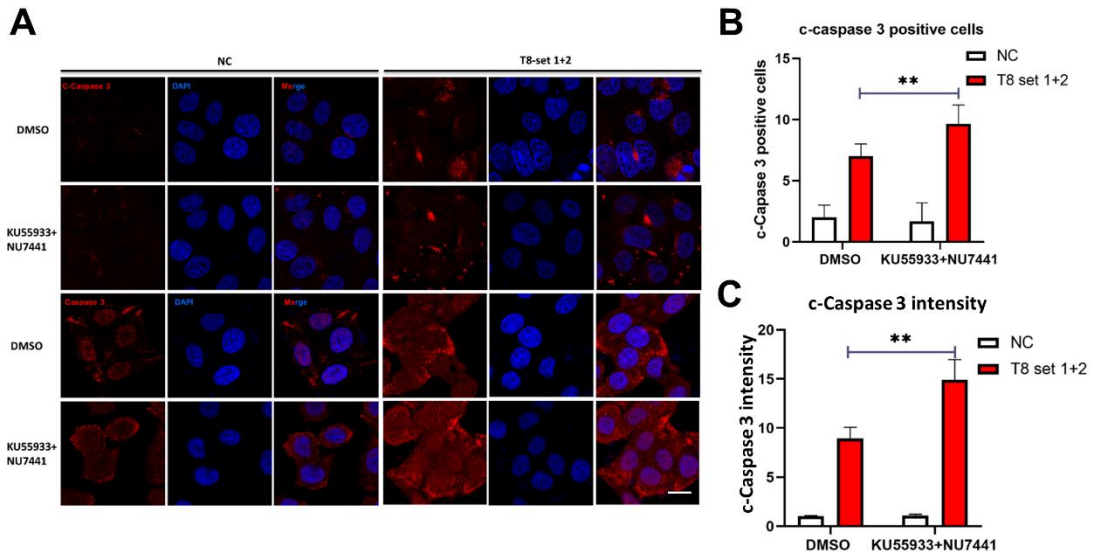
70 **A.** Representative images of γ H2AX foci in HepG2 cells at 48 h after
 71 transfection with three groups of gRNAs together with Cas9. Scale bar, 20 μ m.

72 **B.** Quantitative analysis of the γ H2AX foci number in the different groups
 73 indicated above. *P<0.05. **P<0.01.

74 **C-F.** At 0, 24, 48, and 72 h after gRNA transfection, cells were pretreated with
 75 DMSO (C), KU55933 (D), NU7441 (E) and KU55933+NU7441 (F), and cell
 76 viability was determined with a CCK-8 assay at OD450.

77

78



79

80

81 **Figure S4. Targeted induction of DSB resulted in apoptosis in cancer cells**
 82 **carrying specific mutations.**

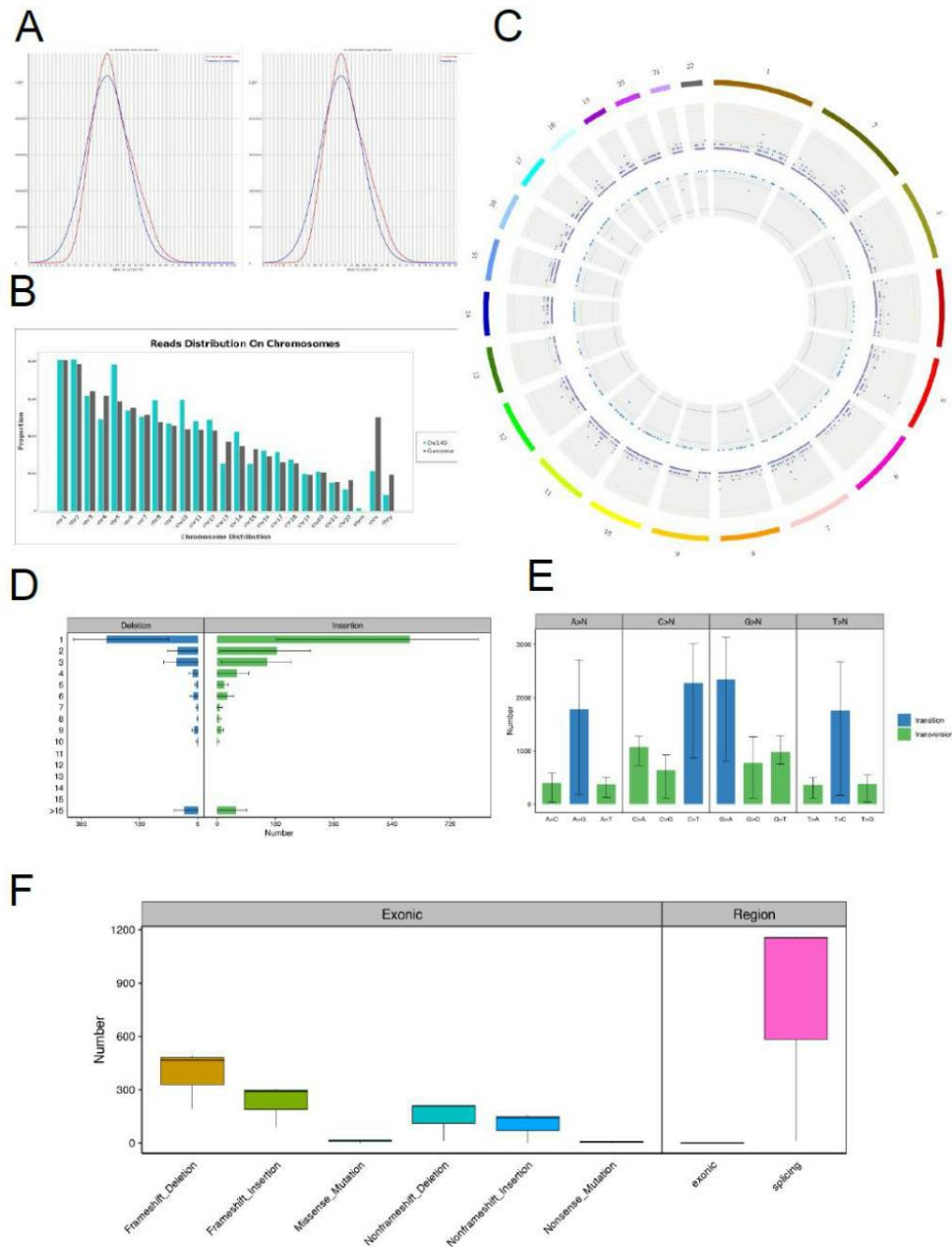
83 **A-C.** representative images and quantitative analysis of cleaved Caspase 3
 84 (c-Caspase 3) in T8 gRNAs&Cas9 introduced group with/without DNA damage
 85 repair treatments (KU55933+NU7441). Scale bar, 20 μ m. *P<0.05. **P<0.01.

86

87

88

89



90

91 **Figure S5. WGS results in DU145.**

92 **A.** Sequence GC Content in DU145 discovered by WGS (whole genome
93 sequencing).

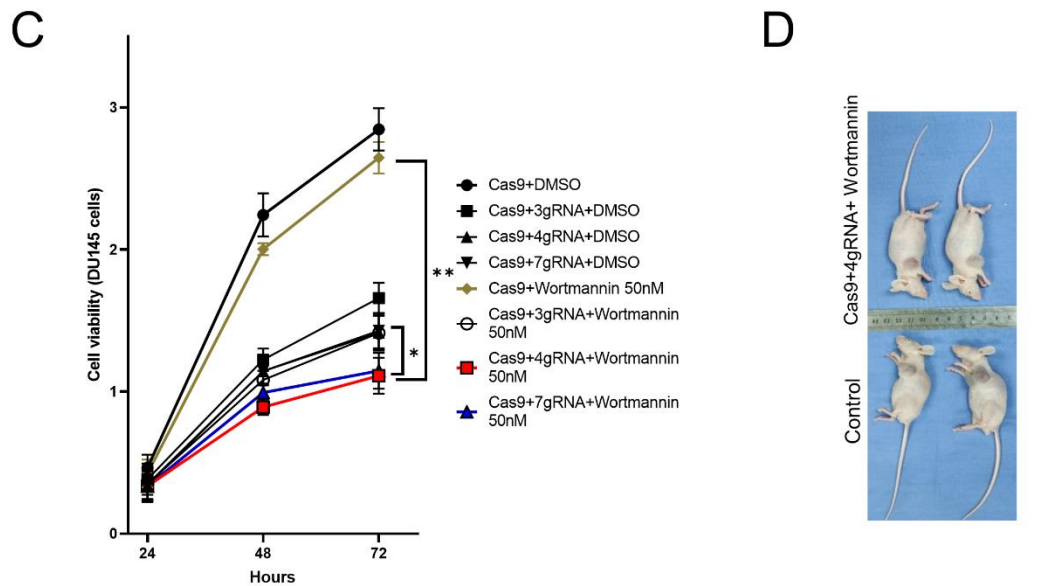
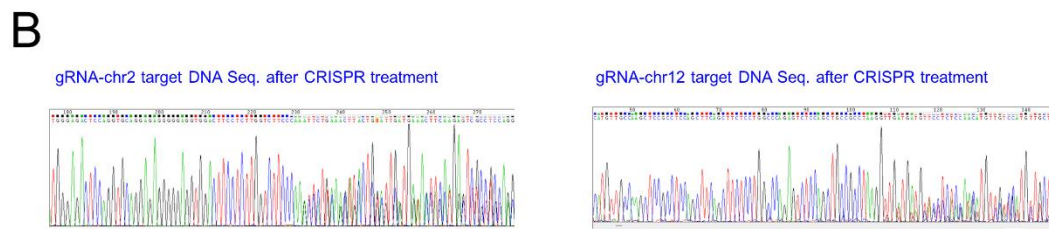
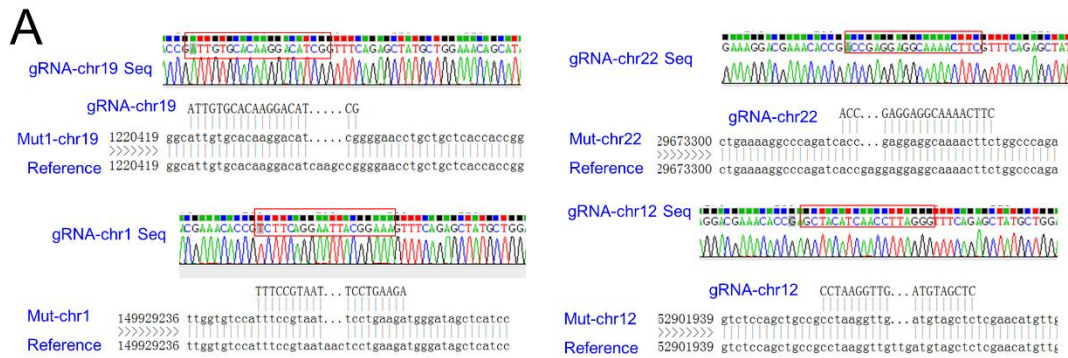
94 **B.** Reads distribution on chromosomes in DU145 discovered by WGS.

95 **C.** A Circos plot showing the genomic landscape of in our cultured DU145 cells
96 discovered by WGS. The outer ring shows chromosome ideograms. The bars
97 along each inner ring represent mutation events.

98 **D.** WGS results showed the substitution of indel (insertion or deletion)
99 in our cultured DU145 cells.

100 **E.** SNP substitution in our cultured DU145 cells discovered by WGS.

101 **F.** WGS results showed the distribution of indel on different DNA segments in
102 our cultured DU145 cells.



103

104

105

106

107

108

109

110

111

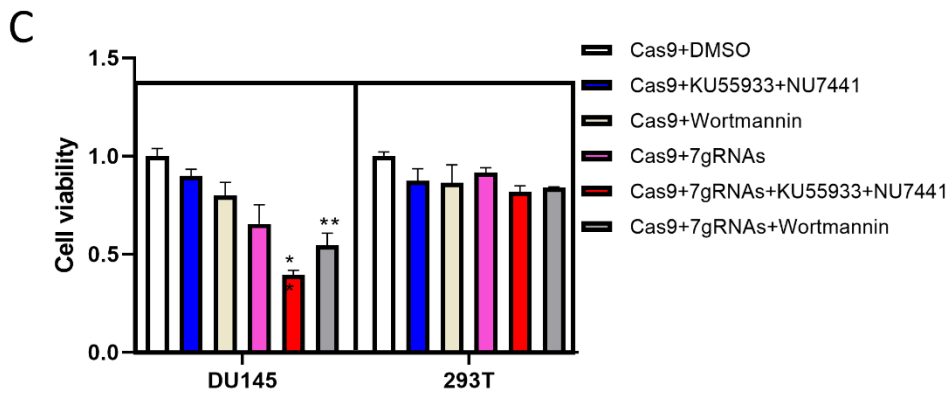
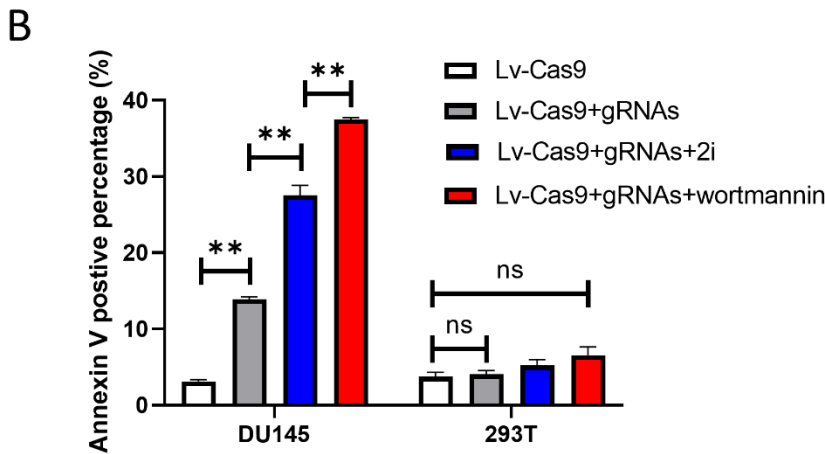
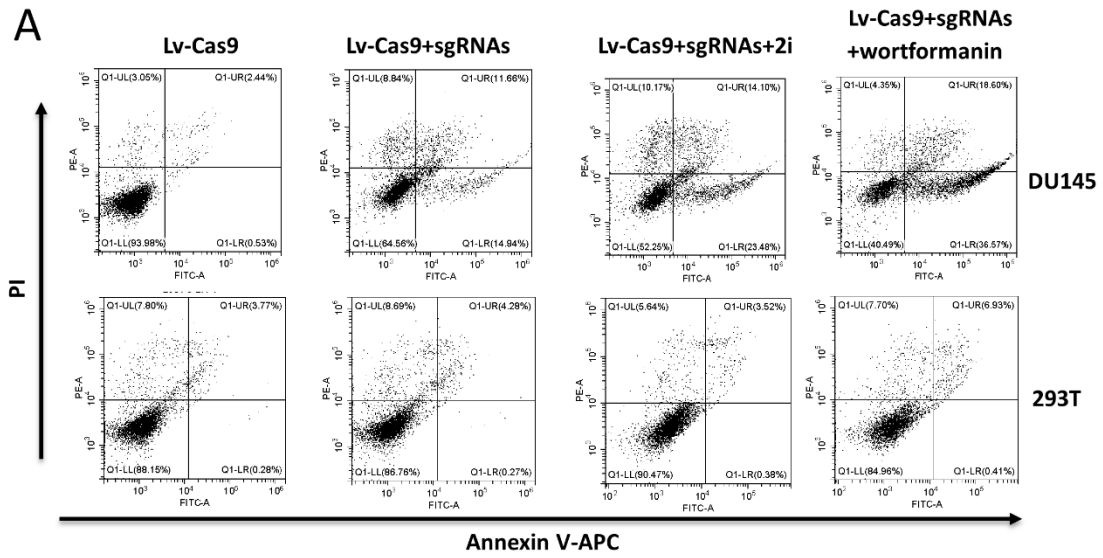
112

113

Figure S6. The "i-CRISPR" strategy could suppress DU145 cell viability.
A. The representative sequences of the designed gRNAs which only target mutated DNA sites in Prostate cancer cells DU145.
B. Representative Sanger sequencing results of the PCR product of Cas9 and gRNA introduced DU145 cells showed the emergence of abnormal peaks at the gRNA targeting sites, which indicated the designed CRISPR could successful induce DSBs in cells.
C. CCK-8 assay results of cell viability of DU145 cells after the treatment of Cas9 and different combinations of gRNA-expressing lentiviruses and Wortmannin (50nM).

114 D. Xenograft experiments showed decreased growth of DU145 cells after
 115 4gRNAs-Cas9 and Wortmannin treatment in nude mice.

116
 117



118

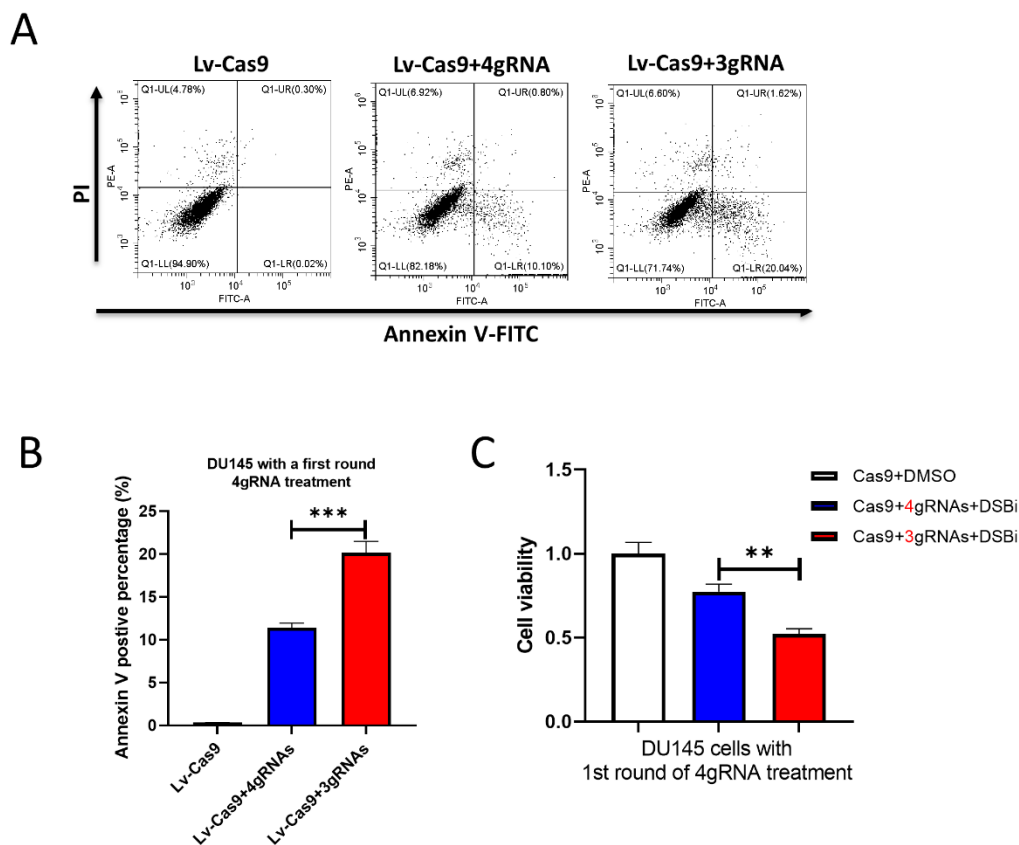
119 **Figure S7. The "i-CRISPR" strategy could induce cell death in DU145**
 120 **cancer cells but not normal 293T cells.**

121 **A.** Representative of cell apoptosis in DU145 cells transfected with a gRNAs
 122 combined treatment with DNA damage repair inhibitors. A lv-cas9 was used as
 123 a negative control. And NU7441+KU55933 and wortmannin was used as DSB
 124 inhibitors. A normal 293T cells without the relative cutting sites were used to
 125 determine the specificity of this strategy.

126 **B.** Quantification of apoptotic cells from different groups were shown. **P<0.01
 127 Vs the relative group.

128 **C.** DU145 cells and 293T cells transfected with lv-cas9, or lv-cas9 plus sgRNAs,
 129 and treated with DNA damage repair inhibitors. After 72h later, cell viability was
 130 measured in DU145 cells and 293T cell with a CCK-8 assay.

131
 132



133

134 **Figure S8 CRISPR targeting new targets could overcome the possible**
 135 **drug resistance problems of our strategy.**

136 **A.** To test the possible resistance of the strategy, DU145 were treated with a
 137 first round of 4 gRNAs mediated CRISPR cutting. Then the survived cells were
 138 subjected to the same 4 gRNAs or a different group of 3 gRNAs cutting. Cell
 139 apoptosis were measured with flowcytometry assay. Representative of cell
 140 apoptosis in DU145 cells transfected with two round of gRNAs was shown in
 141 Fig. S7A.

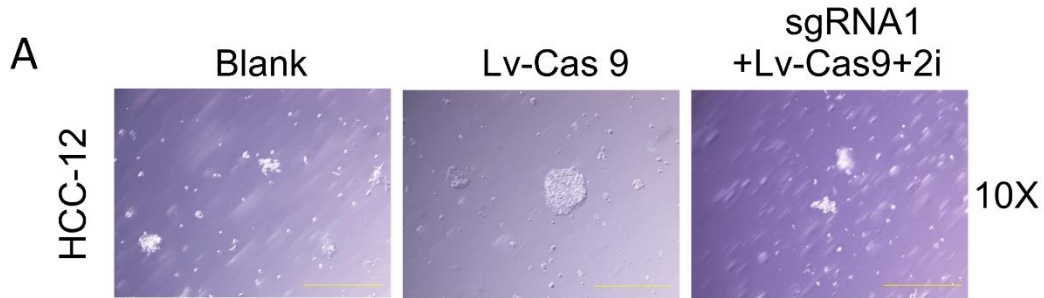
142 **B.** Quantification of apoptotic cells from different groups were shown.
143 ***P<0.001 Vs the 4gRNAs group.

144 **C.** Cell viability was measured with CCK-8 assay in DU145 cell treated with two
145 rounds of CRISPR cutting treatments. **P<0.01 Vs the 4gRNAs group.

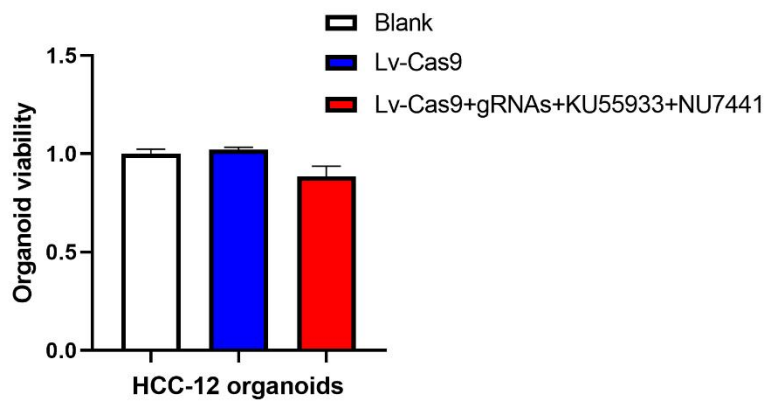
146

147

148



B



149

150 **Figure S9. The "i-CRISPR " strategy could only specifically suppress HCC**
151 **organoid with the designed mutations.**

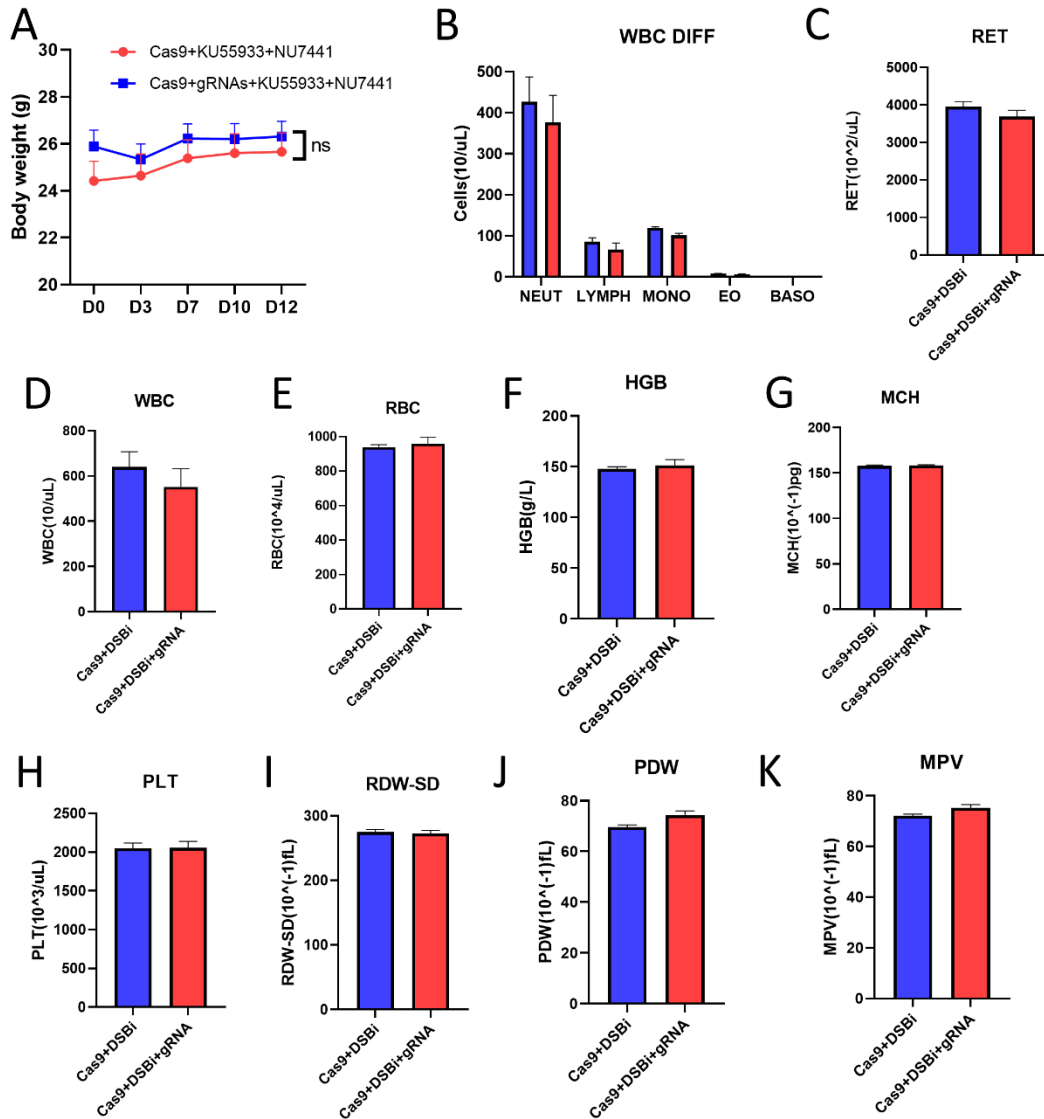
152 **A.** Representative images of organoids (HCC-12) transfected with cas9 and/or
153 gRNAs (HCC-227) combined with DNA damage repair inhibitor treatment.

154 **B.** The viability of organoids was measured with a CCK-8 assay.

155

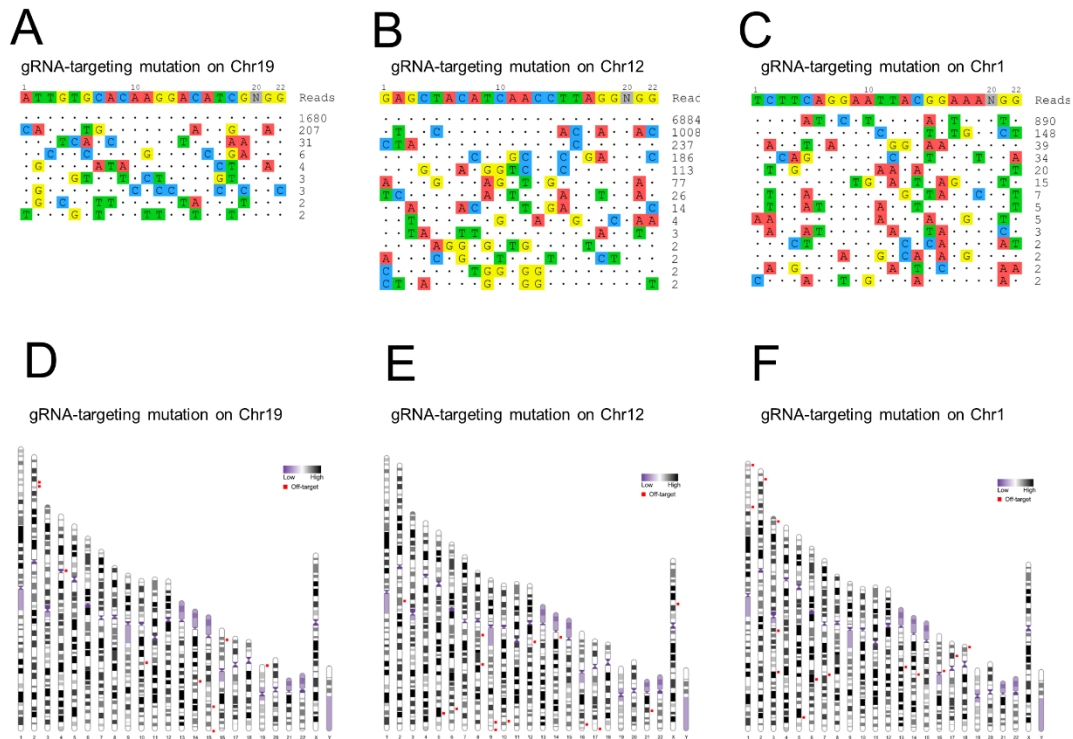
156

157



158
 159
 160
 161
 162
 163
 164
 165
 166
 167
 168
 169

Figure S10. The "i-CRISPR " strategy could not significantly affect the weight, blood routine and other biochemical indicators of PCa PDX mice.
A. The body weight of PDX bearing mice were recorded every three days after the injection of gRNA and DSB inhibitor.
B-K. The blood routine test and biochemical parameters were measured on D12 after the application of CRISPR cutting strategy. No significant difference was observed in the two groups.



170

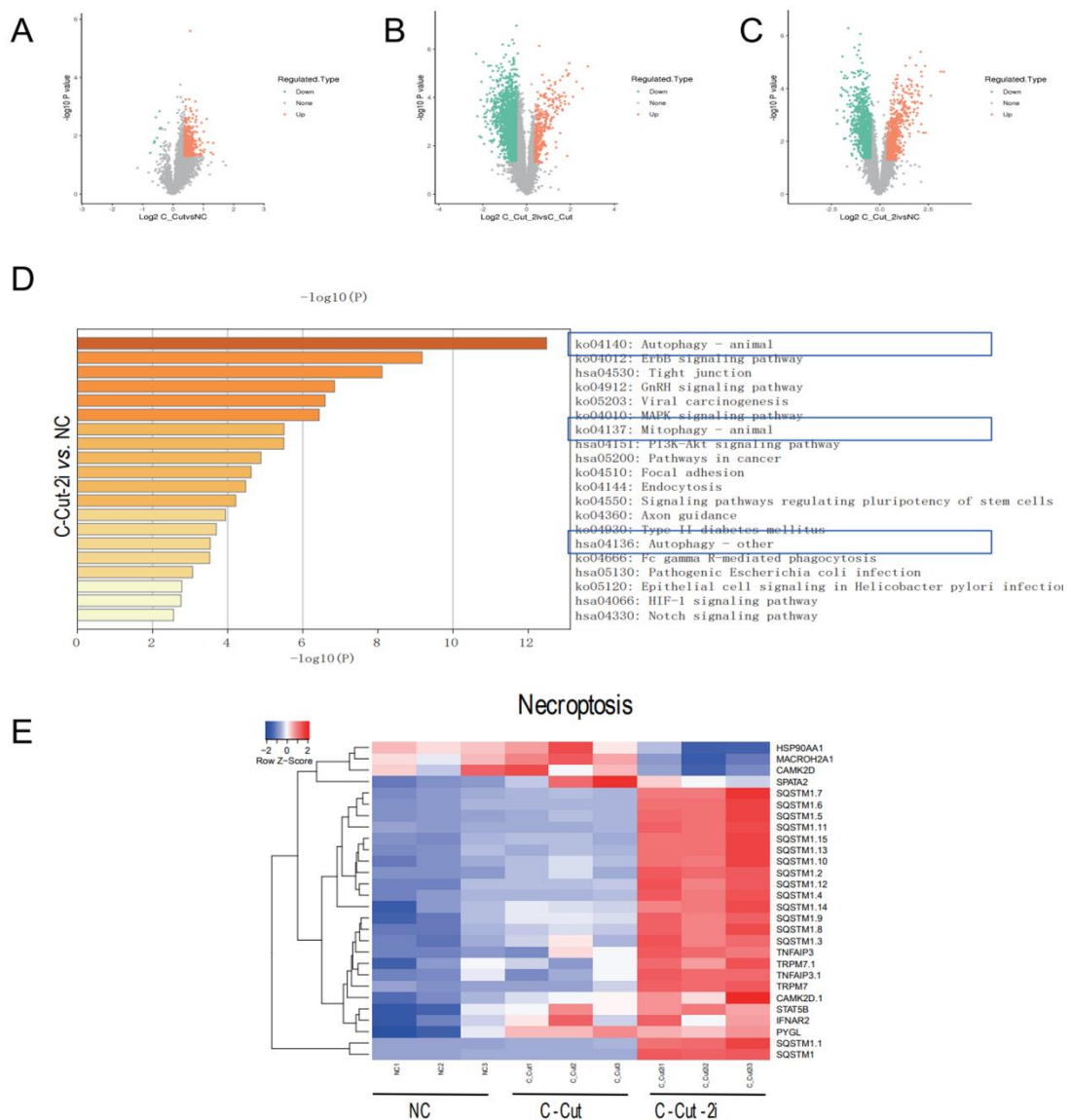
171 **Figure S11. Sequences of off-target sites identified by GUIDE-seq for the**
 172 **mixture of Cas9 and 3 gRNAs targeting mutated sites and treated DU145**
 173 **cells.**

174 **A-C.** On-target and off-target efficiencies with gRNA targeting the mutation
 175 located on Chr19 (A), Chr12 (B) and Chr1 (C) evaluated using GUIDE-seq.

176 **D-F.** Off-targets distributions on all the chromosomes with gRNA targeting the
 177 mutation located on Chr19 (D), Chr12 (E) and Chr1 (F) evaluated using GUIDE-
 178 seq.

179

180



181

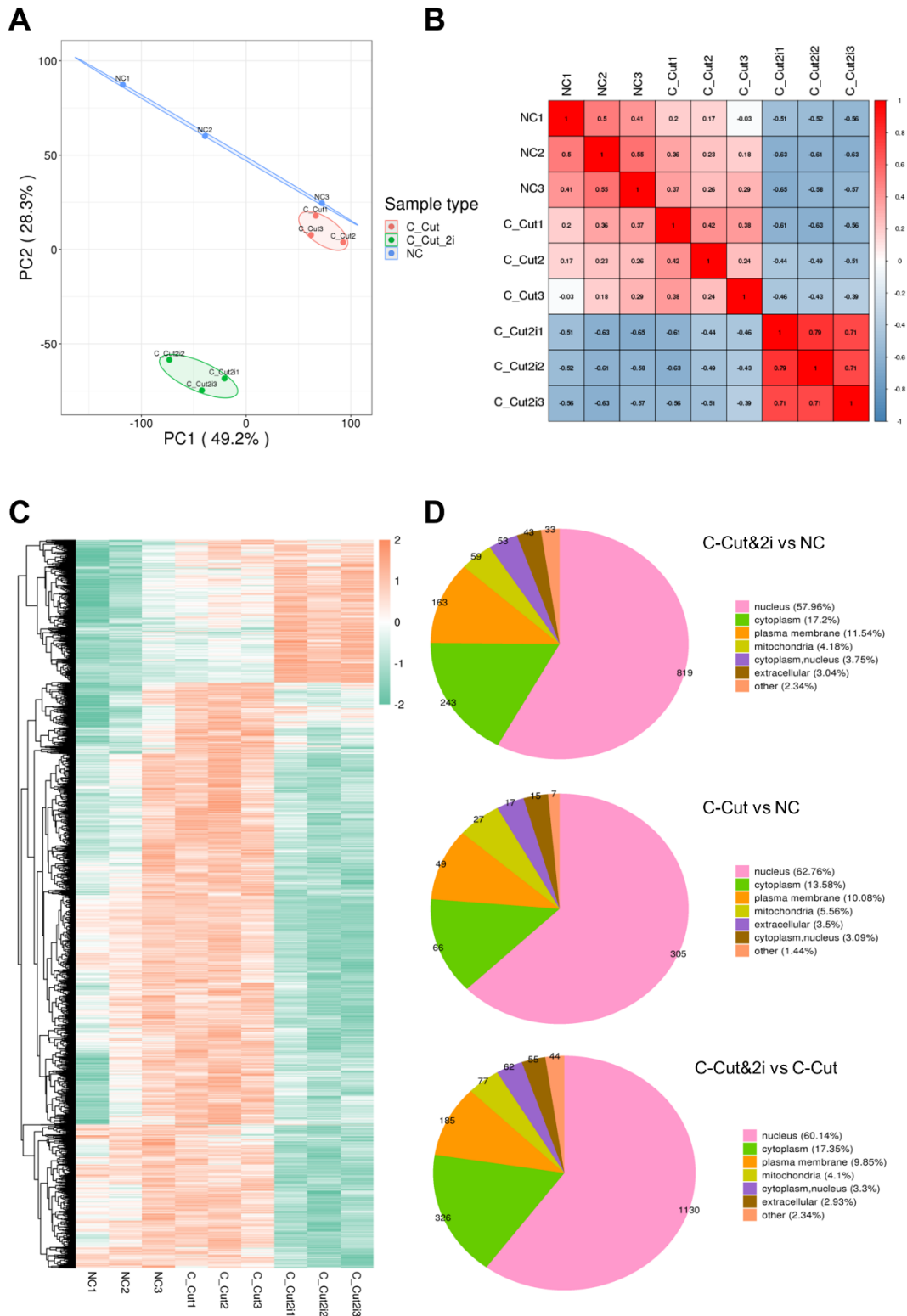
182 **Figure S12. Quantitative phosphoproteomics analysis elucidate the**
 183 **molecular mechanism of the "i-CRISPR" strategy in HepG2 cells**

184 **A-C.** Volcano plot shows differentially phosphorylated proteins between the C-
 185 Cut and NC groups (A), C-Cut-2i and NC groups (B), and C-Cut-2i and C-Cut
 186 groups (C) after quantitative phosphoproteomics analysis using tandem mass
 187 spectrometry. NC: negative control, only treated with Cas9; C-Cut: CRISPR-
 188 Cut, treated with Cas9 and the 8 gRNAs in the T8 set; C-Cut-2i, CRISPR-Cut
 189 treated with the T8 set and 2i (NU7441 and KU55933).

190 **D.** Enrichment of GO terms for the proteins with upregulated phosphorylation
 191 between the C-Cut-2i and NC groups.

192 **E.** Heatmap shows the selected differentially phosphorylated proteins related
 193 to necroptosis among the 3 groups.

194

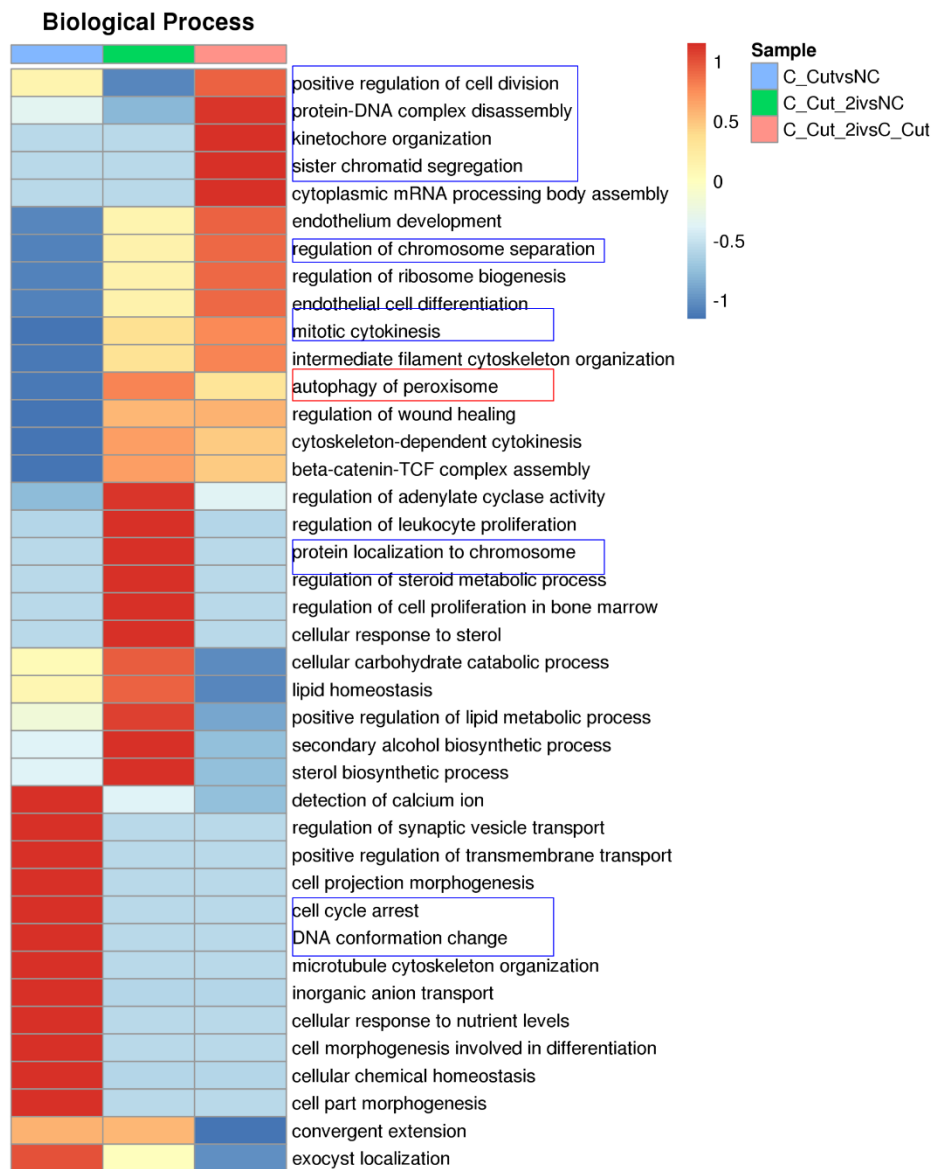


195

196 **Figure S13 Differentially phosphorylated proteins analysis after the "i-**
 197 **CRISPR" strategy treatment.**

198 **A.** The principal component analysis (PCA) result of the 9 samples (each group
 199 has 3 samples) after quantitative phosphoproteomics analysis using the
 200 Tandem Mass. NC: negative control, only treated with Cas9; C-Cut: CRISPR-

201 Cut, treated with Cas9 and 8gRNAs in the T8 set; C-Cut&2i, CRISPR-Cut with
 202 T8 set and 2 inhibitors (NU7441 and KU55933).
 203 **B.** Pearson correlation coefficients between all samples are shown in Heatmap.
 204 **C.** Heat map shows the landscape of differentially phosphorylated proteins
 205 among the 3 groups.
 206 **D.** Pie chart shows the distribution of differentially phosphorylated proteins in
 207 cell components based on GO analysis.
 208



209
 210 **Figure S14 Enrichment of GO terms for differentially phosphorylated**
 211 **proteins among the 3 groups.**

212 Enrichment of GO terms for differentially phosphorylated proteins among the 3
 213 groups after quantitative phos-phoproteomics analysis using the Tandem Mass.
 214 NC: negative control, only treated with Cas9; C-Cut: CRISPR-Cut, treated with
 215 Cas9 and 8gRNAs in the T8 set; C-Cut&2i, CRISPR-Cut with T8 set and 2
 216 inhibitors (NU7441 and KU55933).

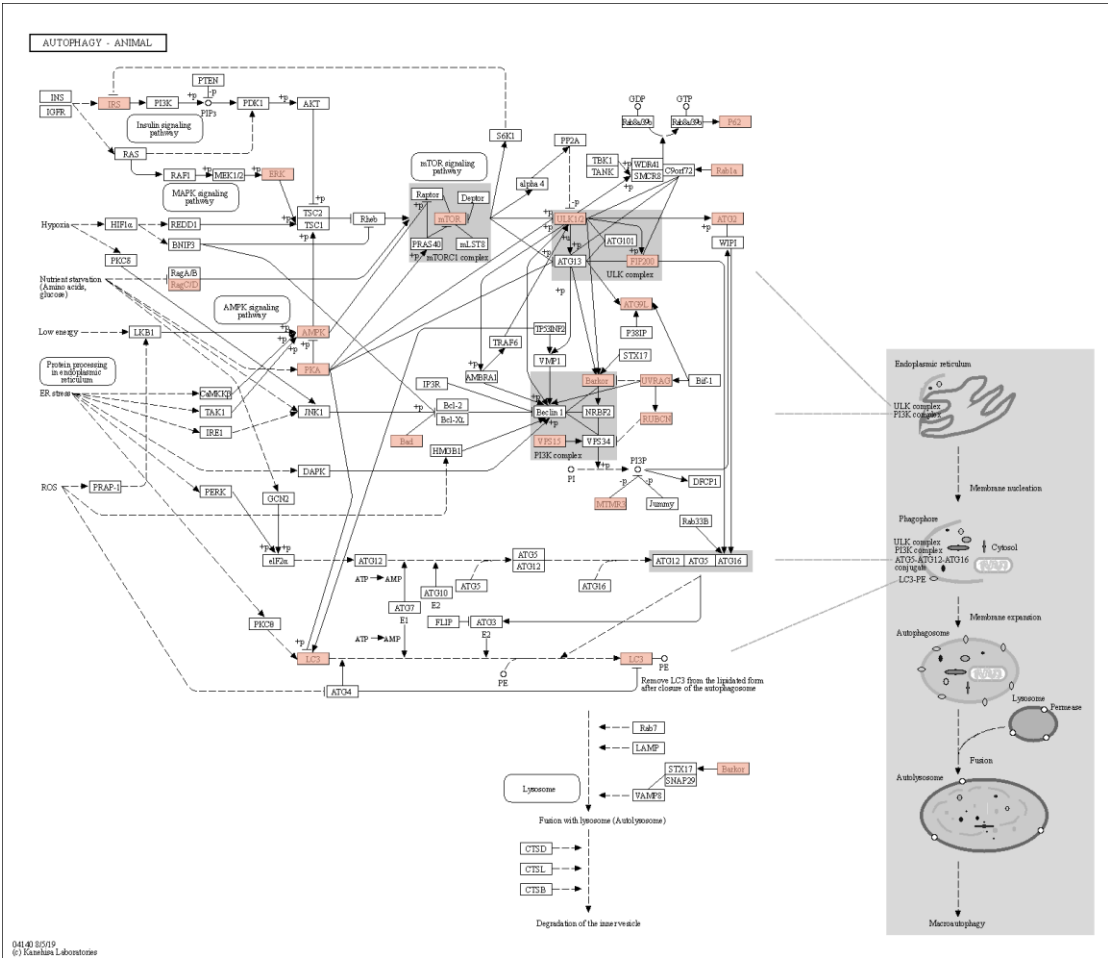
217

218

Differentially phosphorylated proteins between C-Cut-2i vs NC

Other known key proteins in Autophagy-Animal pathway

219



220

221

222 **Figure S15. Activation of autophagy may play a critical role in the molecular**
 223 **mechanism for the increased cell death of our strategy-part 1**

224 KEGG pathway of the enriched term “Autophagy-Animal” in GO analysis, and
 225 differentially phosphorylated proteins are highlighted in the C-Cut-2i vs NC.
 226 Differentially phosphorylated proteins were analyzed using the Tandem Mass.
 227 NC: negative control, only treated with Cas9; C-Cut-2i, CRISPR-Cut with T8
 228 set and 2 inhibitors (NU7441 and KU55933).

229

230

231

232

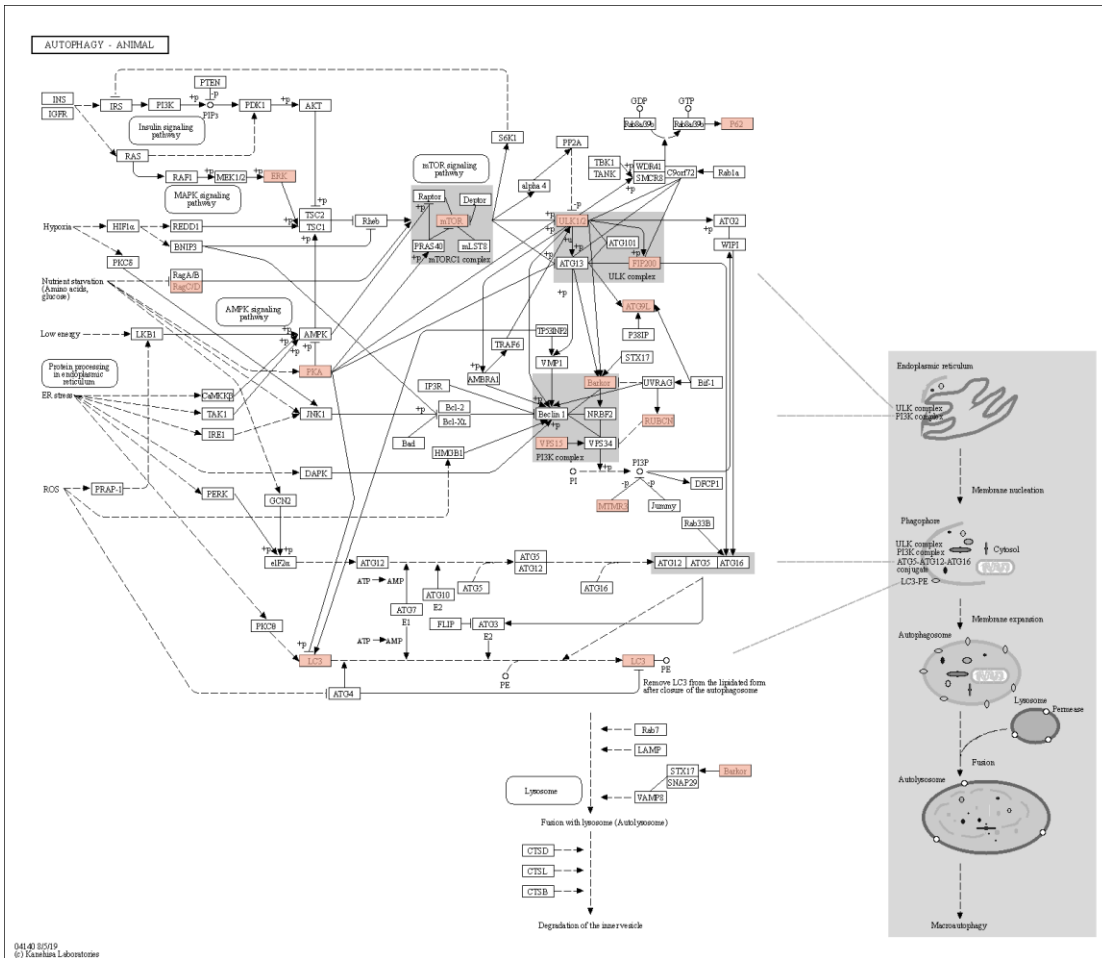
233

234

235

236

237



238

239

240 **Figure S16. Activation of autophagy may play critical role in the molecular**
 241 **mechanism for the increased cell death of our strategy-part 2**

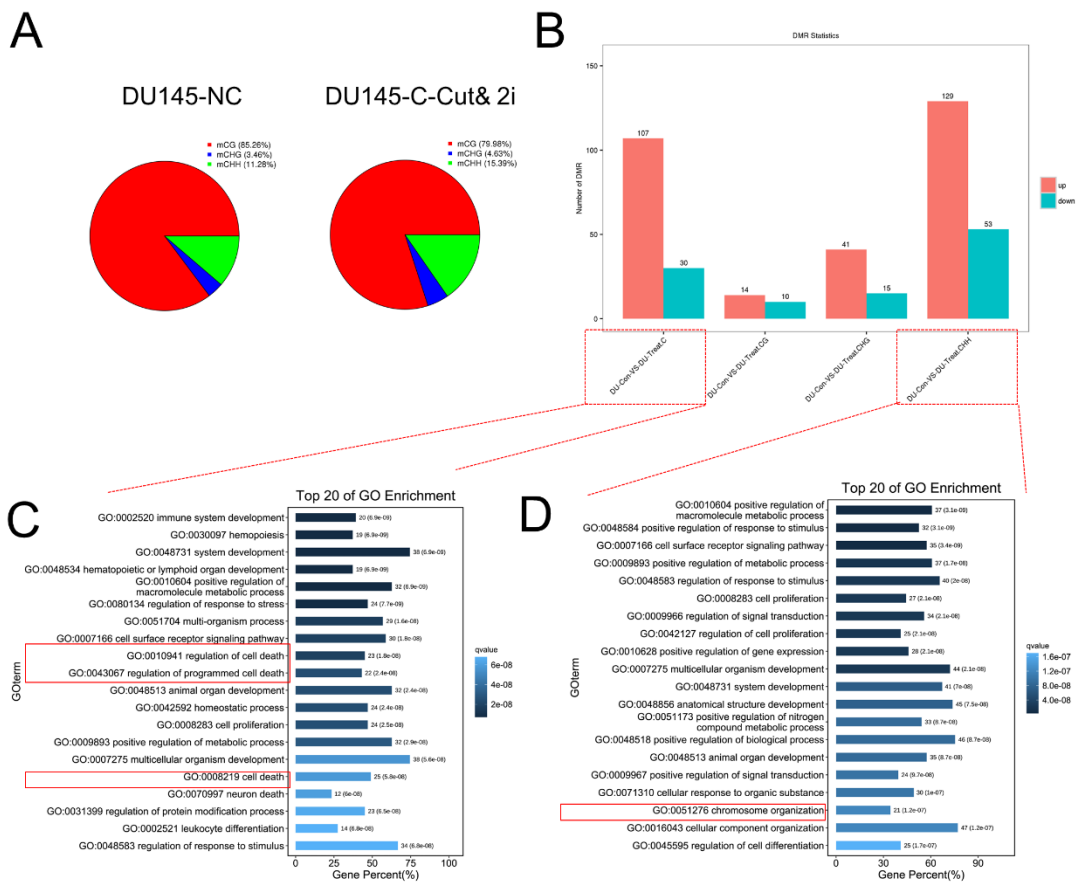
242 KEGG pathway of the enriched term “Autophagy-Animal” in GO analysis, and
 243 differentially phosphorylated proteins are highlighted in the C-Cut-2i vs C-Cut.
 244 Differentially phosphorylated proteins were analyzed using the Tandem Mass.
 245 C-Cut: CRISPR-Cut, treated with Cas9 and 8gRNAs in the T8 set; C-Cut-2i,
 246 CRISPR-Cut with T8 set and 2i (NU7441 and KU55933).

247

248

249

250



251

252 **Figure S17 DNA methylation analysis in control and treated DU145 cells.**

253 **A.** Pie chart shown the change of the composition ratio of methylation levels of
 254 CG, CHG, and CHH contexts in the two groups of DU145. NC: negative control,
 255 only treated with Cas9; C-Cut&2i, CRISPR-Cut with 7gRNAs and 2 inhibitors
 256 (NU7441 and KU55933).

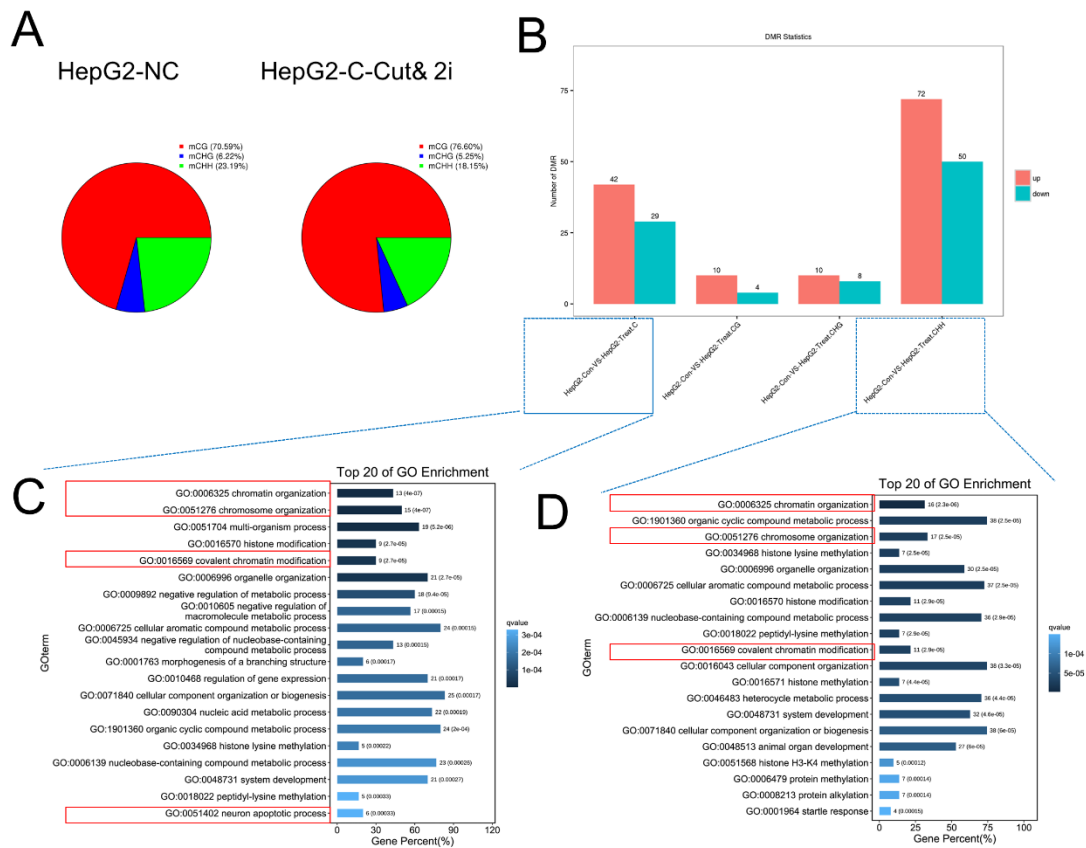
257 **B.** differentially methylated regions (DMRs) numbers of the two comparison
 258 groups. DU-con:Du145 cells only treated with Cas9; DU-treat: Du145 cells
 259 treated with Cas9 and 7gRNAs (CRISPR-Cut and 2 inhibitors (NU7441 and
 260 KU55933));

261 **C.** Enrichment of GO terms for the genes located on the differentially
 262 methylated regions (DMRs) of C between the two comparison groups.

263 **D.** Enrichment of GO terms for the genes located on the differentially
 264 methylated regions (DMRs) of CHH between the two comparison groups.

265

266



267

268

269 **Figure S18 DNA methylation analysis in control and treated HepG2 cells.**

270 **A.** Pie chart shown the change of the composition ratio of methylation levels of
 271 CG, CHG, and CHH contexts in the two groups of HepG2. NC: negative control,
 272 only treated with Cas9; C-Cut&2i, CRISPR-Cut with 8gRNAs and 2 inhibitors
 273 (NU7441 and KU55933).

274 **B.** differentially methylated regions (DMRs) numbers of the two comparison
 275 groups. HepG2-con: HepG2 cells only treated with Cas9; HepG2-treat:
 276 HepG2 cells treated with Cas9 and 8gRNAs (CRISPR-Cut and 2 inhibitors
 277 (NU7441 and KU55933);

278 **C.** Enrichment of GO terms for the genes located on the differentially
 279 methylated regions (DMRs) of C between the two comparison groups.

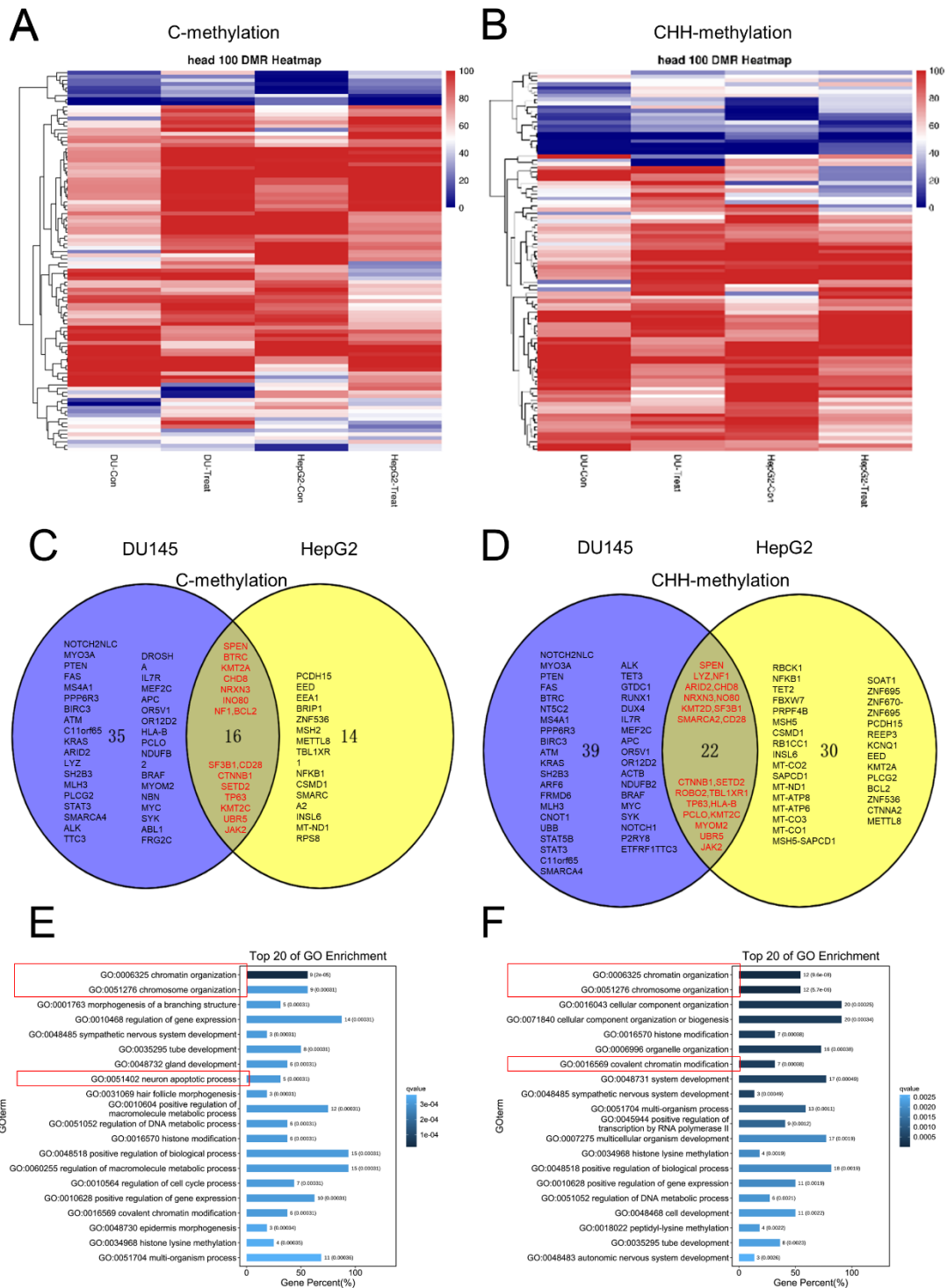
280 **D.** Enrichment of GO terms for the genes located on the differentially
 281 methylated regions (DMRs) of CHH between the two comparison groups.

282

283

284

285



286

287 **Figure S19 Joint analysis of the DNA methylation data in DU145 and**
 288 **HepG2 cells.**

289 **A.** Heat map shown the of the regional methylation rate of the top 100 DMRs
 290 of C. DU-con: DU145 cells only treated with Cas9; DU-treat: DU145 cells
 291 treated with Cas9 and 7gRNAs CRISPR-Cut and 2 inhibitors (NU7441 and

292 KU55933); HepG2-con: HepG2 cells only treated with Cas9; HepG2-treat:
293 HepG2 cells treated with Cas9 and 8gRNAs (CRISPR-Cut and 2 inhibitors
294 (NU7441 and KU55933);

295 **B.** Heat map shown the of the regional methylation rate of the top 100 DMRs
296 of CHH.

297 **C.** Venn diagram shows the common and specific DMRs of C located genes in
298 DU145 and HepG2. Genes in the intersection are genes have DMRs of C in
299 both DU145 and HepG2.

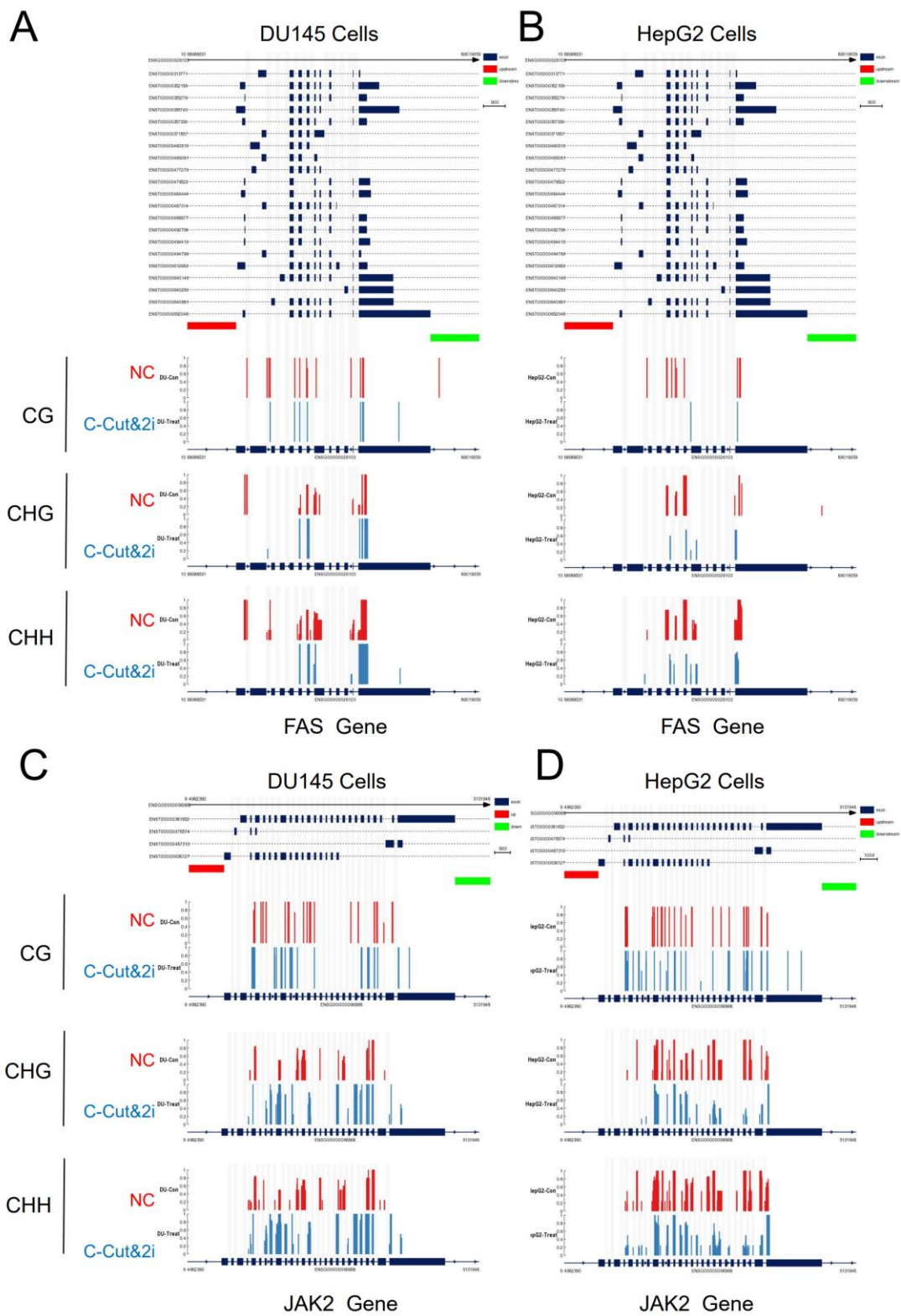
300 **D.** Venn diagram shows the common and specific DMRs of CHH located genes
301 in DU145 and HepG2. Genes in the intersection are genes have DMRs of CHH
302 in both DU145 and HepG2.

303 **E.** Enrichment of GO terms for the genes (in the intersection of C) that have
304 DMRs of C in both DU145 and HepG2.

305 **F.** Enrichment of GO terms for the genes (in the intersection of D) that have
306 DMRs of CHH in both DU145 and HepG2.

307

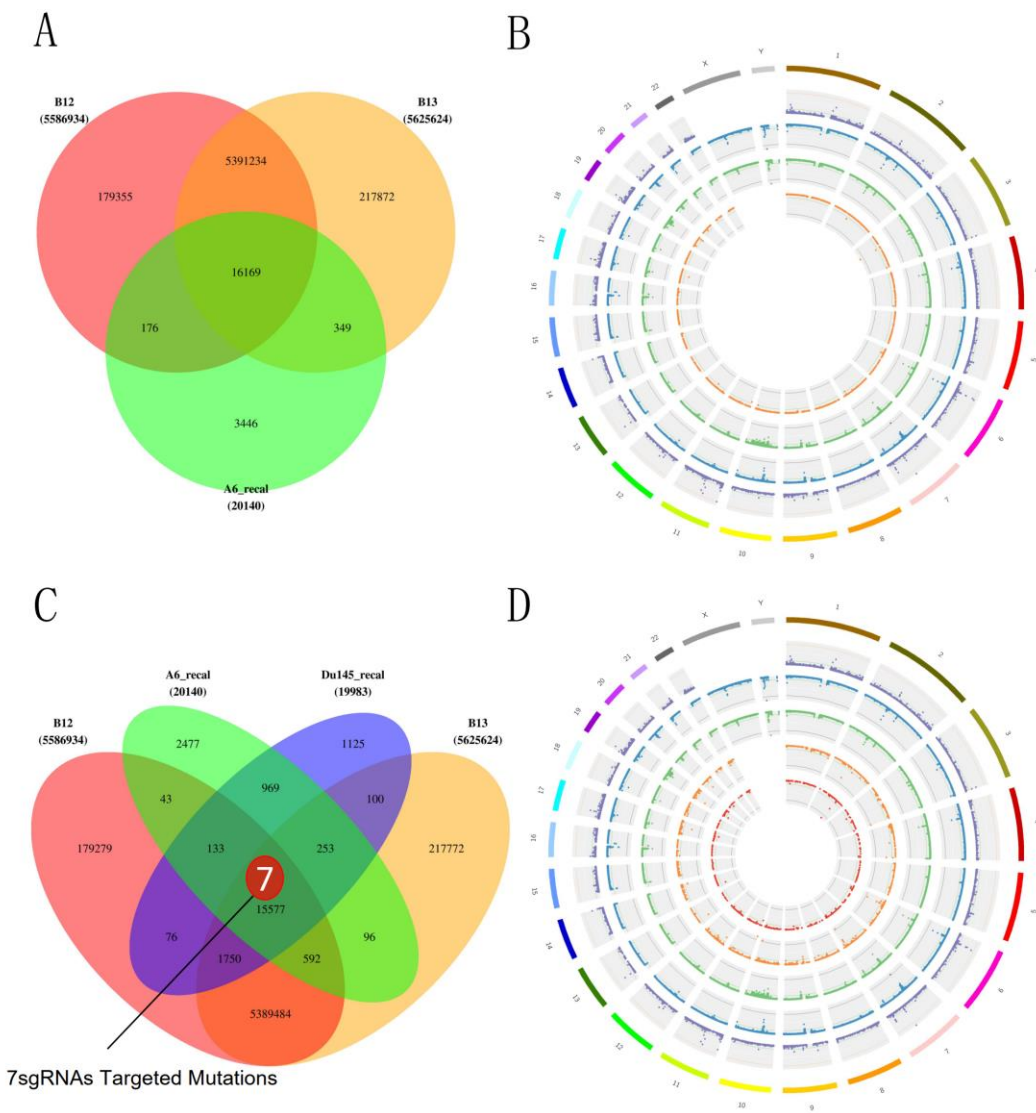
308



310

311 **Figure S20** Gene body region methylation of representative DMR located
 312 genes in DU145 and HepG2 cells.

313 **A.** IGV software depicts the methylation of FAS gene body region in two groups
 314 of DU145 cells.NC: negative control, only treated with Cas9; C-Cut&2i ,
 315 CRISPR-Cut with 7gRNAs and 2 inhibitors (NU7441 and KU55933).
 316 **B.** IGV software depicts the methylation of FAS gene body region in two groups
 317 of HepG2. NC: negative control, only treated with Cas9; C-Cut&2i, CRISPR-
 318 Cut with 8gRNAs and 2 inhibitors (NU7441 and KU55933).
 319 **C.** IGV software depicts the methylation of JAK2 gene body region in control
 320 DU145(DU-Con) and gRNA and 7 gRNAs-Cas9 treated DU145(DU-Treat).
 321 **D.** IGV software depicts the methylation of JAK2 gene body region in control
 322 HepG2(HepG2-Con) and gRNA and 8 gRNAs-Cas9 treated HepG2(HepG2-
 323 Treat).
 324
 325



326

327

328 **Figure S21 Whole-genome sequencing results of DU145 and the 3 DU145**
 329 **derived single cells (A6 , B12, B13) cultured in our laboratory**

330 **A.** Venn diagram shows the common and specific mutations in the 3 DU145
331 derived single cells (A6 , B12, B13) discovered by whole genome sequencing
332 (WGS). A6 is a single-cell clone derived from DU145 that has been cultured
333 alone for approximately 60 passages in our laboratory. From outside to inside:
334 common and specific mutations in B12, B13 and A6. A6 is a single-cell clone
335 derived from DU145 that has been cultured alone for approximately 60
336 passages in our laboratory. B12 and B13 are two single-cell clones derived from
337 DU145 that has been cultured alone for approximately 80 passages in our
338 laboratory.

339 **B.** Circos plot showing the distribution of the common and specific mutations in
340 B12, B13 and A6. From outside to inside: common and specific mutations in
341 B12, B13 and A6.

342 **C.** Venn diagram shows the common and specific mutations in DU145 and the
343 3 DU145 derived single cells (A6 , B12, B13) discovered by WGS. From
344 outside to inside: common and specific mutations in B12, B13 and A6.

345 **D.** Circos plot showing the distribution of the common and specific mutations in
346 DU145, A6, B12, and B13. From outside to inside: common and specific
347 mutations in B12, B13, A6 and DU145.

348

349

350

351

352

353 **2. Supplementary materials and methods**

354 **Materials and methods**

355 **DNA sequencing and CRISPR-Cas9 gene editing**

356 The WGS (whole genome sequencing) and was conducted by OE Biotech Co.,
357 Ltd. (Shanghai, China). TruSeq Nano DNA LT Sample Preparation Kit (Illumina,
358 San Diego, CA, USA) was used for DNA libraries construction. Illumina
359 sequencing platform HiSeq X Ten platform (Illumina Inc., San Diego, CA, USA)
360 was used for WGS of the libraries. Data analysis was also conducted by OE
361 Biotech Co., Ltd. (Shanghai, China).

362 In our criteria, the sgRNAs were selected manually based on the following
363 criteria: 1. High specificity in tumor cells; 2. Each site including 3 continuous
364 base mutations. 3. For cell lines, the sites were both identified in sequencing
365 and public database, which could be present in early passages of cells and
366 shared by most labs in the world. 4. The length of indel bases were also
367 considered for cutting purpose. For the design of each gRNA targeting the
368 selected specific mutated DNA site in tumor cells, we first uploaded the mutated
369 sequence to the gRNA design website CRISPick
370 (<https://portals.broadinstitute.org/gppx/crispick/public>). Then, we used NCBI
371 BLAST to exclude the gRNA sequences that could target any other human
372 normal genomic DNA loci. Then, the selected gRNA sequence targeting
373 mutation in HepG2, DU145 and Hep3B cells was synthesized and cloned into
374 adenovirus expression vector h9350 (padeno-u6-spgrnav2.0-cmv-sfgfp-p2a-
375 3flag-spcas9, Obio Technology, Shanghai) after U6 promotor. And the plasmid
376 expressing both gRNA and Cas9 was then packaged into adenovirus by Obio
377 Technology, Shanghai. The selected gRNA sequence targeting mutation in
378 DU145 was synthesized and cloned into lenti-virus expression vector H6805,
379 pCLenti-U6-spgRNA v2.0-CMV-EGFP-F2A-BSR-WPRE (Obio Technology,
380 Shanghai) after U6 promotor. And the plasmid expressing gRNA was then
381 packaged into lenti-virus (Obio Technology, Shanghai). The usage of the virus
382 was in accordance with the company's instructions and adenovirus safe use

383 principles. All the target sites as well as gRNA sequences in HepG2 cells,
384 Hep3B cell, DU145 cells, organoids and PDX model were listed in the
385 supplementary tables.

386

387 **Cells and treatments**

388 Human liver carcinoma HepG2 cells, Hep3B cells, Huh-7 cells and prostate
389 cancer DU145 cells were purchased from ATCC (USA). Human embryonic
390 kidney cells were purchased from the ATCC and maintained in our lab. Cells
391 were maintained in DMEM or RPMI1640 medium supplemented with 10% fetal
392 bovine serum at 37°C in a 5% CO₂ humidified incubator. For delivering gRNA
393 and Cas9 into HepG2 cells and Huh-7 cells, cells were infected with adenovirus
394 carrying Cas9 and the designed gRNAs targeting the HepG2 mutated
395 sequences in the following group: 4 Targets set 1 (T4-set 1, mixture of 4 Cas9-
396 gRNAs adenovirus targeting 4 HepG2 mutated sites); 4 Targets set 2 (T4-set 2,
397 mixture of another 4 Cas9-gRNA adenovirus targeting another 4 HepG2
398 mutated sites); 8 Targets set (T8-set, mixture of all the 8 Cas9-gRNA adenovirus
399 targeting all the 8 HepG2 mutated sites) and NC control group (NC, negative
400 control gRNA sequence). For delivering gRNA and Cas9 into DU145 cells, cells
401 were infected with lentivirus in the following groups: 3gRNAs (mixture of 3 gRNA
402 lentivirus targeting 3 DU145 mutated sites), 4gRNAs (mixture of 4 gRNA
403 lentivirus targeting 4 DU145 mutated sites), 7gRNAs (mixture of all the 7 gRNA
404 lentivirus targeting the 7 selected DU145 mutated sites) and NC groups. And
405 another Cas9-expressing lentivirus was added into all 4 groups. For delivering
406 gRNA and Cas9 into Hep3B cells, cells were infected with lentivirus carrying
407 Cas9 and the designed gRNAs targeting 4 Hep3B mutated sequences. To verify
408 the cutting efficacy of the gRNAs, PCR products of specific DNA sites from
409 HepG2 cells introduced with 8gRNAs, DU145 cells with the 7gRNA, and Hep3B
410 cells with the 4gRNAs and Cas9 were subjected to Sanger sequencing with
411 (Applied Biosystems, ABI3730).

412 For inhibition of DNA damage repair in HepG2, adenovirus infected cells were

413 treated with ATM inhibitor KU55933, DNA-PKcs inhibitor NU7441 and the
414 combination of “KU55933+NU7441”. For inhibition of DNA damage repair in
415 DU145, lentivirus infected cells were treated with PI3KK inhibitor Wortmannin.
416 To test the resistance resulted from the first-round treatment, DU145 cells
417 treated with first set of sgRNAs were further treated with the same group of
418 sgRNA or a different set of sgRNA for a second round. At indicated time points
419 after transfection, cells were treated and used for next experiments.

420

421 **Organoids and treatment**

422 As previously described, patient derived organoids (PDO) of hepatobiliary
423 tumor were established before and were applied to test the anti-tumor efficacy
424 of our strategy [1]. Briefly, the organoids were kindly provided from our
425 collaborators Prof. Lei Chen from Eastern Hepatobiliary Surgery Hospital in our
426 university. DNA sequencing were performed in the organoids (HCC227) and
427 targeting sgRNAs were designed. Cells of organoids were plated into 384 well
428 plates and after 3 days culture, organoids were infected with lentivirus
429 expressing only Cas9 protein or Cas9 plus sgRNAs. Then the images were
430 taken with a light microscope every day up to 7 days. Alternatively, CCK-8
431 assay was also used to measure the viability of organoids. Data from three
432 independent experiments were statistically analyzed.

433

434 **Animal experiments and patient derived xenograft (PDX) models**

435 The xenograft experiments were performed using nude mice. As we reported
436 previous, prostate cancer cells DU145 cells were subcutaneously injected into
437 the 4-week-old male nude mice [2]. Each nude mouse received 3×10^6 cells in
438 100 μ l of serum-free medium blended with an equal volume of BD Matrigel
439 Matrix (BD Biosciences). After 3 weeks, the mixture of 4 gRNAs lentivirus
440 targeting 4 DU145 mutated sites (treated group) or NC lentivirus were injected
441 intratumorally with Wortmannin and Cas9-expressing lentivirus. The injections
442 were given every three days for a total of four times. Mice were sacrificed at 6

443 weeks. All procedures were obeying to the Animal Care and Use Committee of
444 the Naval Medical University, Shanghai, China.

445 For PDX model, tumor tissues from patients with prostate cancer were resected
446 surgically and implanted into mice with the technique assistance from Shanghai
447 Lidi Co. Ltd as previously described [3]. Briefly, the tumor tissues were cut into
448 size of 1 to 3 mm and implanted subcutaneously into the flank region of male
449 NOG mice. the engrafted tumor tissues were passaged and implanted into
450 different male NOG mice. At the same time, DNA sequencing were also
451 performed in isolated tumor tissues, based on which the sgRNAs were
452 designed and synthesized. Once the PDX model grew to 50 to 80 mm³,
453 lentivirus carrying sgRNAs and Cas9 were intratumorally injected, together with
454 the DNA damage repair inhibitor (KU55933 and NU7441). The lentivirus
455 combinations were injected every two days for three times. Then the tumor
456 volumes were monitored up to 12 days after CRISPR cutting, and the blood
457 routine examination as well as biochemical analysis were performed. At the end
458 point of observation, tumors were resected and tumor weight were measured.
459 the data were expressed as mean SEM, and statistical analysis were further
460 performed (n=6).

461

462 **Immunofluorescence staining and analysis**

463 Immunofluorescence staining was used to detect γ H2AX foci, the cleaved
464 Caspase 3 and Caspase 3 by using methods described in our previous
465 studies[4, 5]. Briefly, cells were seeded on 22X22mm² cover glasses. After
466 different treatments, cells were fixed in 4% paraformaldehyde for 20 min at
467 room temperature, followed by treatment with 0.5% Triton X-100 for
468 permeabilization. Then the slides were blocked with goat serum and incubated
469 with primary antibodies as follows: γ H2AX S139 (CST, 1:1000), c-Caspase 3
470 (Abcam, 1:500), Caspase 3 (CST, 1:200). Then the fluorescence images were
471 obtained with a Zesis LSM-880 confocal microscope in the State Key
472 Laboratory of Genetic Engineering in Fudan University. Image pro plus (Media

473 Cybernetics) were used to count γ H2AX foci and analyze the fluorescence
474 density.

475

476 **Cell apoptosis**

477 At 48h and 72h after CRISPR-virus infected and treatments with DNA damage
478 repair inhibitors, cells were collected and stained with Annexin V-FITC and PI
479 apoptosis kit according to the manufacture's instructions (Yeasen, Shanghai,
480 China). After Annexin V-FITC and PI double staining, cells were analyzed with
481 a cytoflex flow cytometry (Beckman cytoflex, USA).

482

483 **Cell viability**

484 At 0, 24, 48h and 72h after CRISPR-virus infected and treatments with DNA
485 damage repair inhibitors, cells were stained with CCK-8 solution and cell
486 viability was determined with a BioTech reader at the wavelength of OD450.
487 For organoids experiments, CCK-8 solution was added into the wells with
488 organoid and incubated with 4-8 h, after then the wavelength of OD450 were
489 detected with a plate reader.

490

491 **Phos proteomics**

492 The HepG2 cells were divided into three groups: NC, C-Cut and C-Cut-2i, with
493 three samples in each group. The NC (negative control) group was only treated
494 with Cas9; the C-Cut (CRISPR-Cut) group was treated with Cas9 and 8gRNAs
495 in the T8 set; and the C-Cut-2i (CRISPR-Cut& 2i) group was treated with Cas9
496 and 8gRNAs in the T8 set and 2 DNA damage repair inhibitors (NU7441 and
497 KU55933). After 72 hours of treatment, the cells were harvested and prepared
498 for phos-phoproteome analysis.

499 Briefly, an integrated approach involving TMT kit (Thermo Fisher) labeling, high
500 performance liquid chromatography (HPLC) fractionation, immobilized metal
501 affinity chromatography (IMAC) affinity enrichment, and LC-MS/MS using a Q
502 Exactive™ HF-X Hybrid Quadrupole-Orbitrap mass spectrometer coupled with

503 EASY-nLC 1000 liquid chromatography pump (Thermo Fisher Scientific) was
504 employed to quantify the dynamic changes in the whole phosphoproteome of
505 the three groups of cells. Both methods were performed with the support of
506 PTM-Biolabs Co. Ltd. (310018; HangZhou, Zhejiang, China). Metascape
507 webtool (www.metascape.org) was used to conduct Gene ontology (GO)
508 biological process and Kyoto Encyclopedia of Genes and Genomes (KEGG)
509 pathway analysis, allowing us to visualize the functional patterns of DEGs and
510 conduct statistical analysis.

511

512 **Whole-Genome Bisulfite Sequencing**

513 The HepG2 cells were divided into two groups: NC and C-Cut-2i. The NC
514 (negative control) group was only treated with Cas9, and in the C-Cut-2i
515 (CRISPR-Cut& 2i) group, mixture of the Cas9-gRNA adenovirus targeting the
516 selected 8 HepG2 mutated sites and 2 DNA damage repair inhibitors (NU7441
517 and KU55933) were added into cultured HepG2 cells. Similarly, the DU145 cells
518 were also divided into two groups: NC and C-Cut-2i. The NC (negative control)
519 group was only treated with Cas9, and the C-Cut-2i (CRISPR-Cut& 2i) group
520 was treated with Cas9 lentivirus and mixture lentivirus of the 7 gRNAs and 2
521 DNA damage repair inhibitors (NU7441 and KU55933). Three days after
522 treatment, cells were harvested and genomic DNA was extracted using the
523 QIAamp Mini DNA kit (Qiagen,) according to the instructions. The DNA
524 concentration were detected by NanoDrop spectrophotometer and fragmented
525 into 100-300bp by sonication (Covaris, USA) and purified before end repairing
526 and a single “A” nucleotide adding onto the 3’ end of the blunt fragments. Then
527 the DNA fragments were ligated to methylated sequencing adapters, and were
528 bisulfite converted using Methylation-Gold kit. The converted DNA were
529 amplified and sequenced using Illumina HiSeq™ 2500 and the Data were
530 analysed by Gene Denovo Biotechnology Co. (Guangzhou, China).

531

532 **Off-target detection by Guide-seq**

533 DsODN (200pmol) was transfected into cultured DU145 cells(2×10^6) by
534 Lipofectamine 3000 (Invitrogen), and then Cas9 and gRNA lentivirus targeting
535 3 DU145 mutated sites were added into the cells. Three days after treatment,
536 cells were harvested and genomic DNA was extracted using the QIAamp Mini
537 DNA kit (Qiagen) according to the instructions. Library construction, Guide
538 sequencing and data analysis was performed by GeneRulor Company Bio-X
539 Lab, Guangzhou 510006, Guangdong, China.

540 **Statistical analysis**

541 Data were expressed as the means \pm standard error of mean (SEM). GraphPad
542 Prism 8 software was applied for statistical analysis as previously described.
543 Briefly, one was ANOVA was used for comparison among multiple groups. For
544 comparison between two groups, Student's t test was used. $P < 0.05$ was
545 considered as statistically significant. All the experiments were performed at
546 least 3 independent times.

547

- 548 1. Zhao, Y., et al., *Single-Cell Transcriptome Analysis Uncovers Intratumoral Heterogeneity and*
549 *Underlying Mechanisms for Drug Resistance in Hepatobiliary Tumor Organoids*. *Adv Sci (Weinh)*,
550 2021. **8**(11): p. e2003897.
- 551 2. Xiao, G., et al., *The Long Noncoding RNA TTTY15, Which Is Located on the Y Chromosome,*
552 *Promotes Prostate Cancer Progression by Sponging let-7*. *Eur Urol*, 2019. **76**(3): p. 315-326.
- 553 3. Yang, G., et al., *Integrative Genomic Analysis of Gemcitabine Resistance in Pancreatic Cancer*
554 *by Patient-derived Xenograft Models*. *Clin Cancer Res*, 2021. **27**(12): p. 3383-3396.
- 555 4. Lei, X., et al., *Nuclear Transglutaminase 2 interacts with topoisomerase II α to promote DNA*
556 *damage repair in lung cancer cells*. *Journal of experimental & clinical cancer research : CR*, 2021.
557 **40**(1): p. 224.
- 558 5. Liu, L., et al., *Long non-coding RNA ANRIL promotes homologous recombination-mediated DNA*
559 *repair by maintaining ATR protein stability to enhance cancer resistance*. *Molecular cancer*,
560 2021. **20**(1): p. 94.

561

562